

Learning to crawl: benefits and limits of centralized *vs* distributed control

Luca Gagliardi* and Agnese Seminara†

*Machine Learning Genoa Center and Dept of Civil Chemical and Environmental Engineering,
University of Genoa, villa Cambiaso, via Montallegro 1, 16145, Italy*

We present a model of a crawler consisting of several suction units distributed along a straight line and connected by springs. The suction units are rudimentary proprioceptors-actuators, which sense binary states of compression *vs* elongation of the springs, and can either adhere or remain idle. Muscular contraction is not controlled by the crawler, but follows an endogenous, stereotyped wave. The crawler is tasked to learn patterns of adhesion that generate thrust in response to the wave of contraction. Using tabular Q-learning we demonstrate that crawling can be learned by trial and error and we ask what are the benefits and limitations of distributed *vs* centralized learning architectures. We find that by centralizing proprioceptive feedback and control, the crawler leverages long range correlations in the dynamics and ride the endogenous wave smoothly. The ensuing benefits are measured in terms of both speed and robustness to failure, although they come at increased computational cost. At the opposite extreme, purely distributed feedback and control only leverages local information and yield a jerkier and slower crawling, although computationally cheap. Intermediate levels of centralization can negotiate fast and robust crawling while avoiding excessive computational burden, demonstrating the computational benefits of a hierarchical organization of crawling. Our model unveils the trade-offs between crawling speed, robustness to failure, computational cost and information exchange that may shape biological solutions for crawling and could inspire the design of robotic crawlers.

I. INTRODUCTION

All organisms with a distributed nervous system need to coordinate their sensorimotor loop without descending commands from a central nervous system, typical of bilateral animals. Despite the lack of centralized control, many distributed nervous systems reliably manage effective locomotion involving the synchronization of many body parts.

These nervous systems showcase different architectures reflecting varying degrees of distribution *vs* centralization. In cnidarians, the nervous system consists only of diffuse nerve nets and is the most primitive of all animals'. Despite the lack of centralization, cnidaria are capable of complex behaviors. For example, *Hydra vulgaris* achieves highly non-trivial coordination of its body parts to perform somersaults [1]. Furthermore, associative learning in the form of operant conditioning can be induced by either visual or mechanical stimuli for the box jellyfish *T. Cystophora* [2].

Echinoderms, such as starfish, also have a simple radial nervous system consisting of a nerve net of neurons. But while they have no brain, their nervous system is more structured than in the cnidarians, as the nerves connect to a central nerve ring [3]. Starfishes crawl efficiently using hundreds of independent tubular feet which generate robust locomotion without central control. The nerve ring establishes the direction of motion by integrating sensory information detected by the arms [4, 5]. Given the direction of motion, coordination of the tube

feet can emerge purely from a passive mechanical coupling, as showed with a minimal model where behavior of the tube feet is prescribed and no information propagates along the nerve net [6, 7].

Cephalopods, such as octopus, squid and cuttlefish, have evolved a complex nervous system whose size is comparable to that of vertebrates and endows them with impressive cognitive capabilities. They do have a central brain; however most of their nervous system is distributed throughout their arms which are covered in hundreds of suckers that can sense the environment as well as adhere to substrates. Like all soft-bodied animals, these organisms have to coordinate many degrees of freedom to achieve locomotion. For example, octopuses translocate on surfaces by leveraging their taste-by-touch sense, whereby suckers adhere to surfaces and sense them chemically upon contact [8]. The sensory information acquired by the periphery guides suckers' adhesion, yielding displacement of the organism along the surface. However, to what extent locomotion is controlled by the central nervous system *vs* by the ganglia distributed along the arms is not known [9, 10]. Intriguingly, coordination may or may not depend on precise proprioceptive feedback, since the molecular mechanisms for proprioception in cephalopods are unknown [11, 12].

We draw inspiration from these natural crawlers and focus on a toy model to ask what are the pros and cons of centralization *vs* distribution. The crawler is modeled as a collection of suckers distributed along a straight line and connected by springs, and endowed with a rudimentary form of proprioception (extension *vs* elongation of the springs) and a rudimentary form of control of the suckers (adhere *vs* not adhere). Contraction of the springs is not controlled by the crawler but rather follows a stereotyped wave established by a central pattern gen-

* Contact author: luca.gagliardi@edu.unige.it

† Contact author: agnese.seminara@unige.it

erator (CPG). If suckers were to adhere at random times, the crawler center of mass would be unable to move on average: is it possible to learn a pattern of adhesion that enables net translocation?

To answer this question we develop a simulator of the crawler and let it learn to translocate by trial and error using the Q-learning Reinforcement Learning algorithm. We compare the learnability, performance and robustness of centralized *vs* distributed learning architectures. Despite the rudimentary proprioception and control, we find that the sole existence of a common reward –here the speed of the center of mass– is sufficient for independent suckers to learn crawling. When all suckers are simultaneously controlled by a single agent, crawling is both faster and more robust to failure, partially overcoming the crawler’s poor sensorimotor ability. However, the computational cost of the central control scales exponentially with the number of suckers and springs. We then introduce a shallow hierarchical architecture where control is centralized in few control centers. We find that this partial centralization achieves nearly optimal performance and robustness with a limited increase in computational burden. These results complement previous work that focus on controlling contraction rather than adhesion with either purely centralized [13] or purely distributed [14] architectures as well as works where crawling emerges from prescribed control patterns, rather than learning (see e.g. [6, 15]).

We hope that our work will serve as a benchmark to explore the optimal level of centralization in more realistic scenarios for natural and artificial crawling, where constraints on efficiency, robustness and computational costs will all concur to define optimality.

II. MODEL AND LEARNING

A. The 1D crawler model

The model, illustrated in fig. 1, is strongly inspired by the one proposed in [15] and considers the crawler as a series of blocks connected by springs along the body axis. The crawler is placed on a flat substrate and its dynamics is dictated by the springs and the interaction with the substrate. We assume friction is proportional to the sliding velocity of the blocks, akin to a viscous term. Each block can actively modify its viscous coefficient thus playing the role of a sucker. In most of the results we assume the friction coefficients are either 0 or infinite. The blocks move via an elongation-contraction wave that propagates from the tail to the head of the crawler. We assume that the CPG is controlled independently and is unaffected by the blocks/suckers. Note that when all suckers are controlled by a single agent, it is possible to learn the contraction patterns for coordinated crawling without assuming a CPG, as shown in Ref. [13].

Suckers are labeled by their ID n , where $n = 1, \dots, N_s$ and N_s is the number of suckers. The n -th spring is

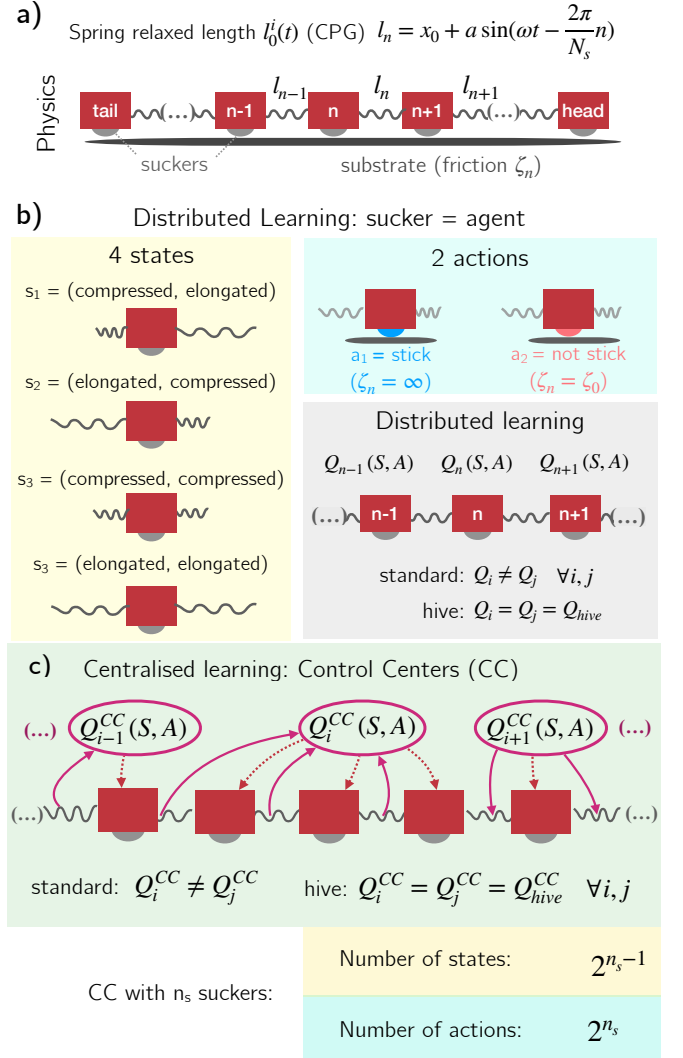


FIG. 1: a) Sketch of the 1D crawler model. b) Sketch of the distributed architecture, including the 4 states available to each agent (individual sucker), the 2 actions the sucker controls and the 4×2 Q-matrix for each sucker. c) Centralized architecture: one or more Control Center (CC) control a subset of contiguous suckers. The states for each CC correspond to all combinations of compression/elongation states of the springs within the CC; the actions are all combinations of adhesion/no-adhesion of suckers within the CC. For multiagency (whether the individual agents are suckers or CCs), the “hive update” corresponds to forcing all agents to agree, i.e. write and read the same Q matrix.

defined as the one to the right of the n -th sucker, and its equilibrium position is given by the CPG:

$$l_n = x_0 + a \sin(\omega t - kn) \quad (1)$$

where $k = 2\pi/N$ with N the periodicity, ω the angular velocity, a a constant and uniform amplitude, and x_0 the natural length of the spring. This latter parameter fixes

the spatial scaling of the model. Here we fix $N = N_s$, so that the wavelength λ corresponds to the length of the crawler L . Arbitrary values of the periodicity are considered in Appendix C, where we show how N alters the importance of each sucker when a crawling strategy is played. To mathematically define the possibility of adhesion by the suckers, we assume that each sucker has a distinct linear viscous coefficient, ζ_n . As detailed in [15], without coordinated adhesion of each sucker/block, the crawler just oscillates along its center of mass and the average velocity is zero. We assume that each friction coefficient can have an identical constant value ζ_0 (no adhesion) or $\zeta_n \rightarrow \infty$ (the n th sucker adheres). The choice of infinite adhesion is one of the ingredients distinguishing our model from [15] where calculations are conducted under the assumption that individual suckers only slightly perturb their friction coefficient. In Appendix A we show the details of the physical model and its parametrization and scaling. In the following, to compare crawlers of different lengths, we will express velocities in normalized units $v \rightarrow v/x_0$ so that the results are independent of spatial scaling x_0 .

1. Expected qualitative behavior from the idealized continuous infinite crawler

In Ref.[15] the authors find an analytical solution for the velocity of the center of mass assuming that the 1D crawler is infinite and approximable to the continuous limit ($x_0 \rightarrow 0$), and that the adhesion is a perturbation. For the sake of clarity we summarize here their results. The perturbation is taken in the form of a traveling wave pulse where only a single sucker can increase its viscous friction at a time, and with the same periodicity and frequency of the CPG (eq. (1)),

$$\zeta(s, t) = \zeta_0(1 + \epsilon p(s, t)) \quad (2)$$

with ϵ a small parameter, and

$$p(s, t) = \sum_{n=-\infty}^{\infty} 2\pi\delta(\omega t - (ks - \beta - 2n\pi) - \Theta) \quad (3)$$

with $\Theta = \tan^{-1} \tilde{\omega}$ and $\tilde{\omega} = \zeta_0 \omega / (k^2 \kappa)$. The extra shift Θ to the CPG of eq. (1) comes from the solution to the unperturbed problem (see eq. (B1), in Appendix B.1), that is, the suckers evolution without adhesion (no net motion of the crawler's center of mass). With these assumptions, they find that the crawling velocity is proportional to

$$\frac{v_{CM}}{x_0} \sim -\sqrt{\omega} \frac{\tilde{N}}{\sqrt{1 + \tilde{N}^4}} \sin \beta \quad (4)$$

with $\tilde{N} = \sqrt{\omega} N / (2\pi)$. Therefore, the optimal positioning of the pulse with respect to the traveling wave has a phase shift of $\beta - \Theta$, with $\beta = 3/2\pi$. At this phase shift and for

a given frequency ω of the CPG, a maximum is expected as a function of the spatial periodicity of the pulse, at

$$N_{\max} = \frac{2\pi}{\sqrt{\omega}} \quad (5)$$

Our model differs from this analytically tractable model in several ways: our crawler is discrete and finite; the head and tail play an important role as discussed below; suckers do not apply a small perturbation to the viscous resistance but rather adhere vigorously to the substrate; finally multiple suckers may adhere at any given moment. In Appendix B we discuss and compare extensively our model and simulator to Ref. [15]. Although we cannot expect quantitative correspondence of our crawler with the analytical model we do find an optimum as a function of the periodicity N , in qualitative agreement with Ref. [15].

B. Learning architectures

In the Reinforcement Learning (RL) paradigm, the learning problem is framed in terms of Environment and Agent. The agent, i.e. the learner, interacts continuously with the environment selecting at each time step an *action* (stick or not stick to the substrate) to which the environment responds with a numerical *reward* and a representation of its *state* [16]. When treating the 1D crawler model as an RL problem, since the task is to achieve unidirectional and fast motion, the reward at each time step is given by the instantaneous center of mass velocity, $R_t = v_{CM}(t)$ when the velocity is positive, and $R_t = -1$ if $v_{CM}(t) < 0$. After several trials, we found this choice to be effective to promote policies maximizing the crawling speed. In order to keep the problem as simple as possible and minimize the requirements on proprioception, we use binary states associated to the spring's tension: 1 = elongated; 0 = compressed. As previously anticipated, actions are also binary and related to each sucker being adhering or not: $\zeta_n = \infty$ or $\zeta_n = \zeta_0$, respectively. Learning can be achieved via several algorithms. We here use standard tabular Q-learning, where a *quality matrix*, or Q-matrix, is learned with an iterative process. The Q-matrix is used to build a (deterministic) *policy*, consisting in selecting at each state the action that maximizes the empirical *return* which is an estimate of the expected cumulative reward when following the current policy. For a given agent its Q-matrix follows the update rule

$$Q_{t+1}(S, A) = Q(S_t, A_t) + \alpha_t \left[R_{t+1} + \gamma \max_a Q_t(S_{t+1}, a) - Q(S_t, A_t) \right] \quad (6)$$

where α_t is the learning rate at integration step t and γ the discount. The learning parameters α, γ are discussed in the next section. Therefore, the dimensionality of the Q-matrix is given by $|\mathcal{S}| \times |\mathcal{A}|$, with \mathcal{S} and \mathcal{A} the ensembles of states and action, respectively. As illustrated

Architecture	ϵ	lr	minimum training steps \times episode and per agent
Distributed (standard)	$\lesssim 10^{-2}$	$\sim 10^{-3}$	minimum $\sim 50k$ steps ^a
Distributed (hive)	$\sim 10^{-2}$	$\sim 10^{-3}$	$\sim 18k$ step
Centralized (small ^b CC)	$\sim 10^{-2}$	$\sim 10^{-2}$	$\lesssim 100k$ steps, about half for hive
Centralized (large ^c CC)	$\sim 10^{-2}$	$\gtrsim 10^{-1}$	$\gtrsim 100k - \sim 1000k$ steps, about half for hive
Fully centralized (single CC)	$\sim 10^{-1}$	robust up to $\gtrsim 10^{-1}$	$\gtrsim 100k - \sim 1000k$ steps

^a difficult to converge and N_s dependent

^b 5 or 6 suckers per control center.

^c 10 or 15 suckers per control center.

TABLE I: Approximate value of the exploration parameters used for the various architectures, considering different sizes and number of CCs. The precise value is case specific and was tuned manually by considering the trade-off between satisfactory levels of exploration and convergence.

in fig. 1, agency can be defined by the learning architecture in several ways. Each architecture carries a specific definition of states and actions which dictates the dimensionality of the Q-matrix, hence the computational cost. Finally, we assume that each agent can act on temporal scales comparable to the CPG oscillation frequency, so that responses are instantaneous. To investigate the role of centralization *vs* distribution, we explore two families of learning architectures, which we illustrate next.

1. Distributed control

Each sucker is considered an independent agent (panel b of fig. 1). Each agent, excluding tail and head, has 4 states which are all the combinations of the spring states of the neighboring springs and 2 actions. Tail and head of the crawler, have only 2 states since for them one spring is missing. Therefore, each intermediate agent-sucker has a 4x2 dimensional Q-matrix, and tail and head a 2X2 Q-matrix.

2. Centralized control

We introduce centralization by defining an agent as an assembly of several suckers and springs which we call Control Center (CC), as illustrated by panel c of fig. 1. The number of CCs controlling the crawler depends on how many suckers are included in each CC and can range from several CCs down to a single CC, which corresponds to the highest degree of centralization. Centralized architectures control several suckers and springs simultaneously, hence have access to a richer representation of the dynamical state of the crawler, and can realize many more policies than those realizable in the distributed setting. The state of the CC is given by the compression/elongation state of each spring located between the first and last sucker within the CC; while the action of the CC consists of specifying the binary adhesion/no-adhesion instruction for each of the suckers within the CC. Since the CC has access to all combinations of compression/elongation and adhesion/no-adhesion states and

actions, the state-action space scales exponentially as $|\mathcal{S}| = 2^{n_s-1}$ and $|\mathcal{A}| = 2^{n_s}$, with n_s the number of suckers controlled by the given CC (for n_s suckers under a CC there are $n_s - 1$ connected springs). Note that to facilitate comparisons and have the same dimensionality of the Q-matrix for each CC we made the arbitrary choice to ignore the spring between two adjacent CCs.

3. The hive assumption

Whenever multiple agents control crawling, a simplifying assumption may be adopted imposing that all agents learn the same policy. This is the so called *hive* assumption or Population-Based Training [17–19], where a population of agents is used to find a shared solution. In all our multiagent learning schemes –including distributed and centralized with multiple CCs– we compare standard learning to hive learning, as illustrated in fig. 1. In practice, each agent writes and reads the same Q-matrix. The distributed hive Q-matrix becomes a 8X2 tensor, where in addition to the 4 states associated to the internal sucker there are 2 extra entries for the tail, (null,elongated) and (null, compressed), and for the head, (elongated,null) and (compressed,null)¹. For the hive CCs there is no need to modify the Q-matrix between hive and standard learning, since all CCs have Q-matrices that are identical in shape, as discussed above. Clearly, the hive assumption speeds up training as it allows to parallelize the learning process. However, it also affects significantly the learned policies, as all agents are forced to learn the same policy, despite being placed at different locations relative to the propagating wave. In other words, the hive update imposes a consensus mechanism and all agent must “agree” on the same policy. In fact the removing the hive policy we find that different agents will learn distinct policies, and the hive update reduces

¹ Note that in this case the problem is effectively hive only for the internal suckers, whilst tail and head remain genuinely independent (since their states are unique) as in standard multiagent RL.

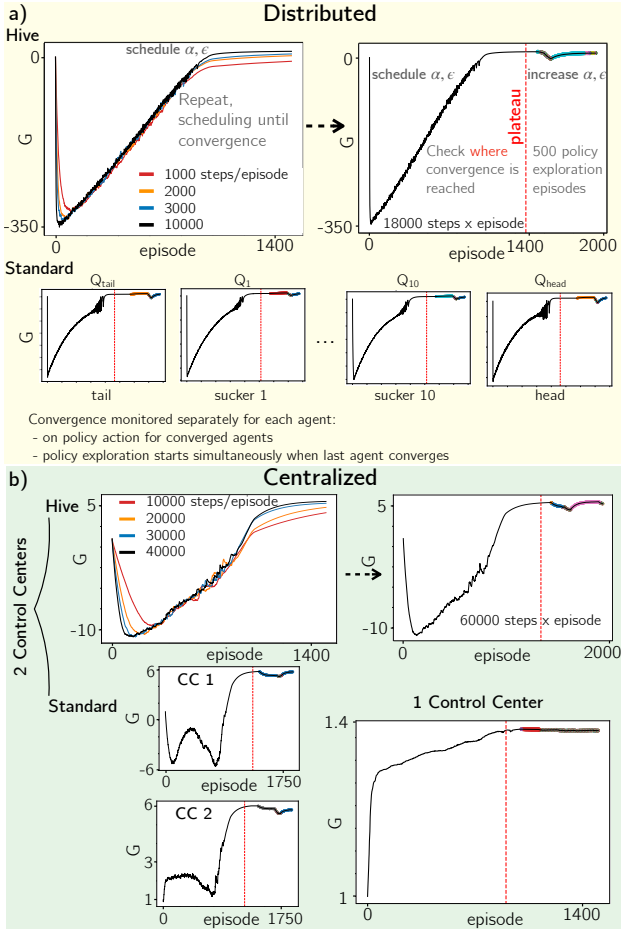


FIG. 2: Illustration of the training protocol on a 12 suckers crawler for various learning architectures. Note that when there are several agents the same procedure is applied to each agent (one Q matrix per agent). In the “exploration” phase, where several (sub-optimal) policies are stored, each color change represents a different policy (see also fig. 5). The specific value of α (learning rate) and ϵ used for exploring sub-optimal policies are case-specific and their order of magnitude is shown in table I.

the number of policies that are learned, as discussed in the Results section.

C. Learning protocol

RL theory and algorithms are extensively covered in specialized books and articles (e.g. [16]). As briefly summarized before, in tabular Q-learning during training we iteratively update the Q-matrix using eq. (6). To keep a certain degree of exploration during training we adopt the standard procedure of following an ϵ -greedy policy, that is, with a finite probability ϵ a random action is chosen instead of the one prescribed by the current policy (i.e. the action maximizing the current estimate of

the value). During training, both the exploration ϵ and learning rate α in eq. (6) are scheduled to decrease linearly, to ensure convergence to a final estimate of Q . Note that convergence to the optimal Q matrix is only guaranteed asymptotically, hence different trainings will lead to different sub-optimal policies, which we explore systematically in the following. In this work the scheduling process starts at a value of $\epsilon_{\max} = 0.9$ and $\alpha_{\max} = 0.1$ and is scheduled down to $\epsilon_{\min} = 0.001$ and $\alpha_{\min} = 0.001$. Inspired by standard episodic RL tasks, we call with the term *episode* any scheduling event of α and ϵ . For episodic tasks, an episode is usually defined by a “termination” after which the agent is reset to another initial state and moves on to the next episode. However, the task explored in this work, which consists in achieving fast and unidirectional motion, is not episodic but *continuing*, since there is no termination. Therefore, here an episode is composed of an arbitrary number of integration steps with the same value of α and ϵ . The discount rate is fixed to $\gamma = 0.99$ to maximize long term reward $G_t = \sum_{k=0}^{\infty} \gamma^k R_{t+k+1}$. For continuing tasks, another possible formulation of the reward is that of *average reward* [16, 20], which does not require discount and where the reward becomes also an estimate. Preliminary results however do not indicate any visible benefits of this formulation in our problem. Note that although the equations of motion are deterministic, our learning problem is stochastic. There are two sources of stochasticity: i. the coarse grained state space and ii. the definition of agents. Both i. and ii. imply that the reward signal is a stochastic variable. Indeed, the speed of the crawler depends on the full dynamical state of the system, defined by the (continuous) speed, position and adhesion of all suckers and on the relaxed length of all springs. However, as per i., our crawler does not observe the full dynamical state of the system, but rather its coarse projection onto discrete binary states of compression vs elongation of all the springs. Thus given the actions of all suckers, the center of mass is not fully determined yielding a stochastic reward $R(t)$. Moreover, in all multiagent architectures each agent is unaware of other agents’ actions, as per ii., hence once again the actions of any individual agent do not individually determine the speed of the center of mass (i.e. the reward). This latter source of noise in the reward is bypassed by the fully centralized architecture with a single control center (1CC).

With this in mind, to monitor progress during learning we considered the average value G , with $G = 1/|\mathcal{S}| \sum_s \max_a(Q(s, a))$, and the average taken over the states. As illustrated by fig. 2, we set an automatic protocol consisting in repeating the learning procedure until a plateau in G is detected: when the plateau is not encountered after 1500 episodes, we repeat the process changing the scheduling by increasing the number of steps per episode. When several Q-matrices are learned simultaneously (for instance, in standard distributed control) the convergence is monitored separately for each agent. Due to the stochastic nature of the problem, we noticed that

repeating the learning procedure yields different policies. Without attempting a systematic analysis of the ensemble of sub-optimal policies, we design a protocol to account for the stochasticity of this learning process. To efficiently store several sub-optimal policies, without repeating the entire training procedure, we introduced the following strategy: when convergence is detected, the learning parameters are raised to a small and constant value and 500 extra episodes are run letting Q evolve accordingly. At each episode the corresponding policy is stored. As reported in table I, the value of α and ϵ for this “policy exploration” phase are set differently according to the learning architecture considered with the purpose of exploring (sub) optimal policies without disrupting significantly the plateau that was reached by G . The value of α and ϵ that is needed to remain in the plateau reflects how robust the optimal policy is to perturbations, and appears correlated to the degree of stochasticity previously discussed. Centralized architectures appear to need stronger exploration of the plateau to “jump” between sub-optimal policies. We find a fairly stable plateau region in the exploration phase of the fully centralized 1 CC architecture even for large values of α and ϵ . This is due to the high degeneracy of this architecture, where many different policies perform similarly, as discussed later (see fig. 5). Finally, we find that the hive update introduces some degree of stabilization of the learning process since we observed the need of less integration steps (as expected) and a smaller sensitivity to scheduling and exploration parameters. The source code for all different architectures is available at [21].

III. RESULTS

Using the learning protocol described above, we store 500 optimized policies for each architecture and quantify performance as the average speed of the center of mass of the crawler for the best 250 policies. We obtained velocities by playing each policy over a trajectory of 20000 steps. In computing the average we accounted for the multiplicity of each policy, so that policies which are found several times will be more represented as well as quasi-degenerate policies realizing similar crawling velocities.

We find that performance for all architectures depends on the number of suckers N_s (fig. 3), qualitatively consistent with the infinite continuous crawler case. Performance peaks for $N_s \approx 12$ and then exhibits a long-range decay beyond the peak (as discussed in Methods, the number of suckers is identical to the spatial periodicity of the CPG wave, N). The position of the peak depends on the physics of the crawler; in the infinite crawler it depends on the wave frequency ω , see eq. (5). To investigate the limits and properties of multiagency and centralization in cooperative/coordinated actions we will focus largely on the peak. We tuned parameters so that the peak occurs at $N_s = 12$, which is computationally

treatable for all learning architectures from the most distributed to the most centralized. Whether and how natural crawlers orchestrate the central pattern generation and the suckers to operate near the peak is a fascinating question for further research.

We find that the tail and head of our finite crawler play a key role, thus distinguishing our problem from the infinite crawler for which an asymptotic solution is available. However, the analytical optimal policy is a useful heuristic for the internal suckers as discussed below. We thus construct a reference heuristic policy prescribing that (i) internal suckers follow the analytical optimal policy eq. (3) with $\beta = 3/2\pi$ from [15] (see [Supplementary Video 1]), and (ii) tail and head anchor in response to negative forces, i.e. the head adheres when it is dragged backward by the elongated spring to its left and the tail adheres when it is pushed backward by the compressed spring to its right. It is important to observe that to implement the heuristic strategy, the simulator prescribes adhesion according to a phase shift, thus measuring time and space. In contrast, because we use binary compressed/elongation spring states, our agents (the suckers, or the CCs) have no access to the CPG’s wave phase. Thus, our simple crawlers cannot implement the heuristic policy, due to their limited states and controls. Intriguingly, our poor state representation can be compensated by a more centralized control which recovers a smooth traveling wave by controlling multiple suckers at a time, as we will see in the following.

A. Distributed control

Let us first focus on distributed forms of control, where each sucker is an agent (fig. 3, left). When suckers play random actions, the center of mass does not move on average, as expected (random policy, green dashed line). If tail and head adhere in response to negative forces, even if the internal suckers perform a random action, the center of mass does move, showing the importance of the crawler’s tail and head (semi-random policy, orange dashed line). If tail and head adhere in response to negative forces and the internal suckers adhere according to the analytical results described above, performance further increases (heuristic benchmark, gray dashed line). Although the optimal policy of the internal suckers is obtained in the infinite continuous crawler limit, the clear improvement of the policy relative to the semi-random policy suggests that away from the boundary, the infinite crawler may be a useful approximation of our finite discrete crawler. When we let agents act according to a policy that has been learned through trial and error, performance is intermediate between the semi random policy and the heuristic benchmark (blue circles and red triangles). We find that standard learning is harder than hive learning, but it achieves better performance and nearly matches the heuristic benchmark described above (e.g. for 15 suckers). As a reminder, in hive learn-

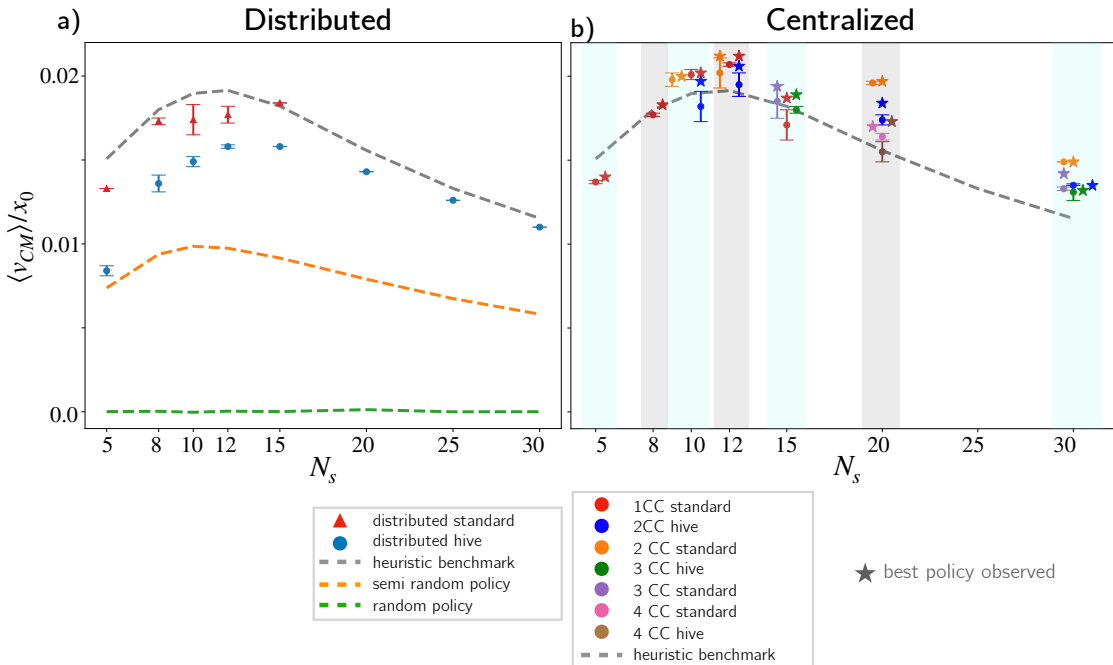


FIG. 3: Average velocity of the crawler center of mass *vs* number of suckers, for different learning architectures. Markers and errorbars correspond to average and standard deviation of performance over the 250 best learned policies for distributed architecture (left) and centralized architectures (right). Colored bands in panel b) group results obtained for the same value of N_s (which have been horizontally scattered for clarity, so symbols do not overlap).

ing all suckers learn the same policy, whereas in standard learning each sucker learns its own individual policy. Almost invariably trainings with hive architectures learn the same policy π_H , regardless of N_s . According to π_H , internal suckers adhere in response to the $\leftarrow | \leftarrow$ state while the tail and head – which are connected to a single spring – adhere in response to the states $\times | \leftarrow$ and $\leftarrow | \times$ respectively. The interpretation of the hive policy π_H is simple: each sucker adheres in response to negative forces, i.e. when all adjacent springs push it backward. For $N_s \geq 15$, all our trainings converge to the same policy π_H , with no suboptimal policies ever learned (hence the absence of the errorbar in fig. 3). The same behavior was found when training distributed hive policies for even larger crawlers with $N_s > 30$ (results not shown) further confirming that π_H is the best consensus policy. Departures from this policy emerge only for small N_s where the specific dynamics of few suckers might affect the global consensus. For $N_s < 15$ trainings converge to a small number of policies; the best learned policy is π_H for $N_s = 5$ and 12, and it is a slightly different policy $\hat{\pi}_H$ only for $N_s = 8$ and 10. π_H and $\hat{\pi}_H$ are almost identical, except internal suckers also adhere in response to the $\rightarrow | \rightarrow$ state, and the tail never adheres. For small number of suckers, $\hat{\pi}_H$ is marginally faster than π_H (e.g. for 10 suckers speed is ≈ 0.017 vs ≈ 0.015). Thus collective hive learning is highly transferrable, in that the hive policy can be applied to crawlers with any number of suckers

with no need for retraining, consistent with previous results obtained with genetic algorithms [14]. Adopting the hive policy results in a clear traveling wave of adhesion, with only one sucker adhering at a time (see animation of the hive policy in [Supplementary Video 2]). Note that, as already remarked above, the individual suckers do not have access to their phase shift, and as a result, this architecture cannot learn a policy that implements our heuristic benchmark. Indeed, this heuristics requires a finer proprioceptive signal, e.g. inferring the phase from the precise intensity of the restoring forces, rather than its sign.

Intriguingly, the standard learning, where each sucker acts according to its own policy, realizes a more complex dynamics with multiple suckers adhering simultaneously and no visible traveling wave of adhesion. In doing so it achieves a more complex group behavior and better performance. Note that, although standard learning achieves better performances, we find that training is more computationally expensive and in our hands was limited to $N_s = 15$: beyond this limit the training did not converge. This is likely due to the intrinsic level of stochasticity: all agents learn simultaneously, but rewards are coupled, as the motion of the tentacle depends on the full dynamical state of the system. Thus good actions may be hard to learn as they may not be individually good enough to yield a positive reward. Moreover, in all cases where standard learning was successful,

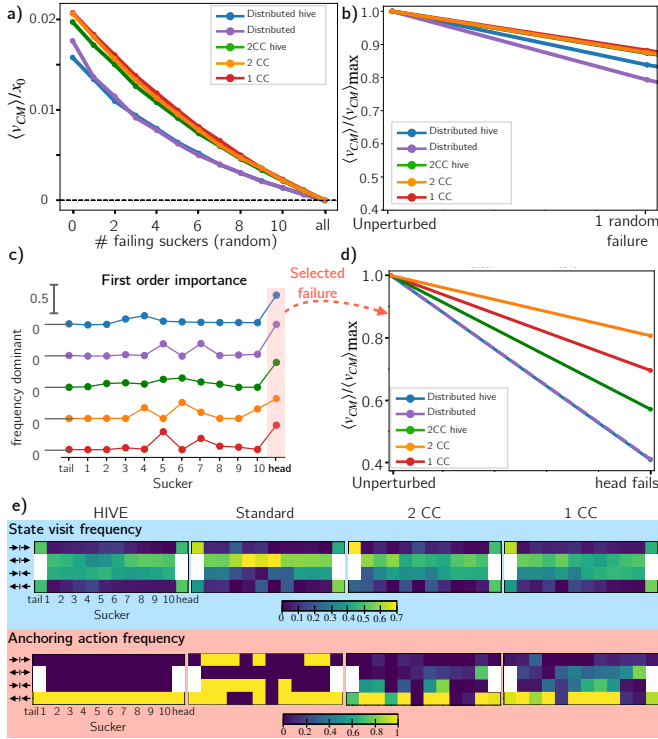


FIG. 4: Robustness analysis of the best policy for 12 suckers crawlers with various learning architectures. a)

Performance (velocity of the crawler) *vs* number of failing suckers. b) Performance of the optimal policy with 1 failing sucker relative to optimal performance with no failing suckers. c) Frequency each sucker is the dominant contributor to the drop in performance in a trajectory, showing that the head is the most important sucker. d) Performance drop due to failure of the head.

e) Statistical behavior of a 12 sucker crawler for different distributed and centralized architectures. Top row: for each sucker (x axis), and each compression state of its adjacent springs (y axis), the color represents the frequency that state was visited while performing the optimal policy. Bottom row: Fraction of time a sucker adheres, colorcoded from purple (always adhere) to yellow (never adhere) for each of the 12 suckers (x axis) and each of the compression states of their adjacent springs (y axis). The blank entries for head and tail represent that these suckers only have access to one spring, hence two compression states (rather than four).

we noticed an extreme sensitivity to the scheduling parameters, with convergence only using about three times the number of steps per episode relative to the hive solution. In contrast, the distributed hive policies were easily learned.

B. Centralized control

Centralized architectures achieve even better performances, at the cost of increased computational burden (fig. 3, right). Indeed, the number of entries in each Q matrix grows exponentially with the number of suckers controlled by the corresponding control center (CC). Given that $n_s \leq N_s$ is the number of suckers controlled by each control center, there are N_s/n_s CCS whose quality matrix has dimensions $|\mathcal{S}| \times |\mathcal{A}| = 2^{n_s-1} \times 2^{n_s}$. Consistently, learning requires considerably longer training (table I) relative to distributed architectures, where training requires to optimize N_s Q-matrices whose dimensions are independent from the crawler size $|\mathcal{S}| \times |\mathcal{A}| = 4 \times 2$.

At the same time, a higher degree of centralization achieves better performance. We find that a single control center dictating the actions of all N_s suckers performs best for $N_s = 10$ and 12, suggesting that long range correlations across the whole crawler are useful, if well orchestrated. However, training of the single CC is extremely complex; it failed beyond $N_s = 15$, because of the sheer size of the quality matrix, and for $N_s = 15$ it underperforms slightly relative to the 3 CCs. Interestingly, multiple CCs achieve almost the same performance as a single control center, and can be trained even with a much larger number of suckers. For example, the reduction in complexity for $N_s = 12$ is quite impressive: the Q-matrix for a single CC has approximately 10^7 entries, whereas it shrinks to about 2000 entries with two control centers. As for distributed learning, hive learning where each CC is forced to learn the same policy is faster than standard learning, but performs slightly more poorly, although the margin is not as impressive as for the distributed control. Next, let us illustrate in more detail the differences between these architectures, focusing on the 12 sucker crawler. For illustrative purposes, the optimal policies for the various learning architectures, both distributed and centralized, are shown for a 12 suckers crawler in [Supplementary Video 3].

C. Robustness

We showed in the previous sections that moving from pure multiagency to some form of centralization improves performance. However, the benefits are not always sizable, e.g. 1CC improves $\sim 17\%$ over distributed standard and $\sim 30\%$ with respect to distributed hive, when considering 12 suckers. At the same time, computational cost grows dramatically and optimal policies become hard to learn. Are there any other benefits to centralized control?

We next show that centralized architectures are considerably more robust to failure of individual suckers. In fig. 4, we focus on the best policy obtained for each architecture for the 12 suckers crawler and test its robustness to failure. To this end, we extract one or more random suckers at each integration step, and let them perform

a random action (adhere or not with the same probability). All other suckers follow the optimal policy, and no extra learning is allowed. Centralized architectures are more robust to failure: their performance drops slower with the number of failing suckers fig. 4(a), with a single random failure eroding less than 10% performance *vs* about 20% for distributed architectures, fig. 4(b). We then asked how robust are these policies to failure of the most crucial sucker. When we make a single sucker fail consistently over time, we find that the head plays the most prominent role in all of our architectures, as its failure contributes the largest drop in performance fig. 4(c). In fact the head is always the dominant sucker when the CPG wavelength, λ , is equal or larger than the crawler length and not otherwise (appendix C). Failure of the head is particularly acute for distributed architectures (60% drop in performance for fully distributed architectures) against much less dramatic drops in centralized architectures (the most robust being the 2CC with a < 20% drop).

To further quantify the distinct policies we measure the frequency that each sucker experiences the four local compression/elongation states of its adjacent springs, as the policy is played over time. The four local states are represented with the symbols $\rightarrow | \rightarrow$; $\leftarrow | \rightarrow$; $\rightarrow | \leftarrow$ and $\leftarrow | \leftarrow$. The local states are visited with frequencies that vary across the different architectures (fig. 4 (e) top row), but the pattern is relatively preserved. This suggests that the underlying physics constrains the spring dynamics considerably, and may partly overshadow differences in the control architecture. In contrast, the average action played by each sucker in its local compression/elongation state varies dramatically across different control architectures (fig. 4 (e) bottom row). In distributed architectures (left panels), suckers play an action that depends only on their local compression/elongation state, hence colors are binary (adhere or not adhere). In contrast, in centralized architecture, a sucker acts in response to the global (albeit binary) state of compression/elongation, and not only in response of its local state. Intermediate colors in the right panels signify that the local compression/elongation state is not enough to determine whether the sucker will adhere or not. Because centralized policies are dictated by global compression/elongation states, they may be more tolerant to failures of individual suckers.

D. Redundancy

To further elaborate on why centralized policies are more robust, we characterize redundancy. Within a given learning architecture, are many sub-optimal policies learned and are they considerably worse than the best policy? Centralized learning converges several times to the optimal policy but also to several fair sub-optimal policies. For instance, the 1CC architecture converges 116 times out of 500 to the optimal policy π_1 , but also

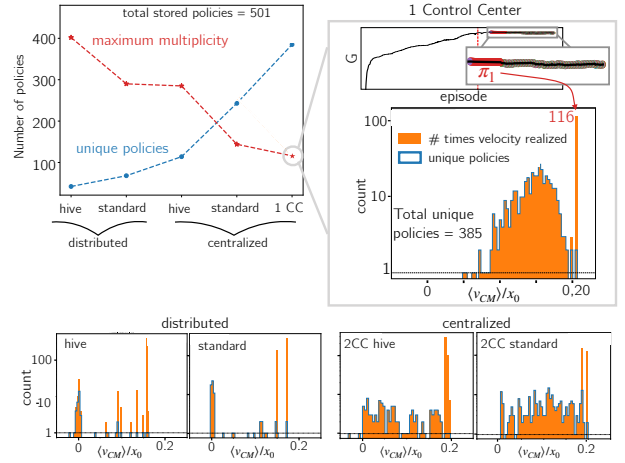


FIG. 5: Distribution of speed for the policies learned by the 12 suckers crawler. Top left: number of distinct policies learned by the 12-sucker crawler with different architectures (blue); number of times the most popular policy was learned (red); Grey inset: detail of policies learned by the fully centralized agent; top: plateau in G , showing the policy π_1 is re-learned several times (same as bottom right panel in Fig 2b); bottom: histogram of the velocities across all 250 policies (orange) compared with the histogram of policies (blue). Bins where the blue histogram is lower than the orange histogram represent that few policies within the bin are re-learned multiple times.

converges to another 384 sub-optimal policies whose performance is only slightly poorer than the optimal performance (fig. 5 top row). Conversely, distributed learning converges even more often to the best policy (large peaks in the histograms in fig. 5 bottom row, corresponding to the best policy) and to fewer considerably worse sub-optimal policies (group of bins near velocity zero). These results suggest that the higher degree of complexity of centralized control offers numerous ways to achieve fast crawling strategies making it harder for the algorithm to spot the best one but at the same time more likely to learn a good policy.

E. Orchestrating a traveling wave

The results described so far suggest that centralized control achieves better performance at the cost of exploring a higher dimensional space of possible states and actions. Why is centralization beneficial? Our crawler is composed of individual suckers that only have the ability to sense a binary compressed/elongated state of their adjacent springs. This makes for a system of poor proprioceptors that do not have access to e.g. their spatial location nor to a clock. We find that by orchestrating the action of many poor proprioceptors, centralized control is able to ride the traveling wave generated by the CPG,

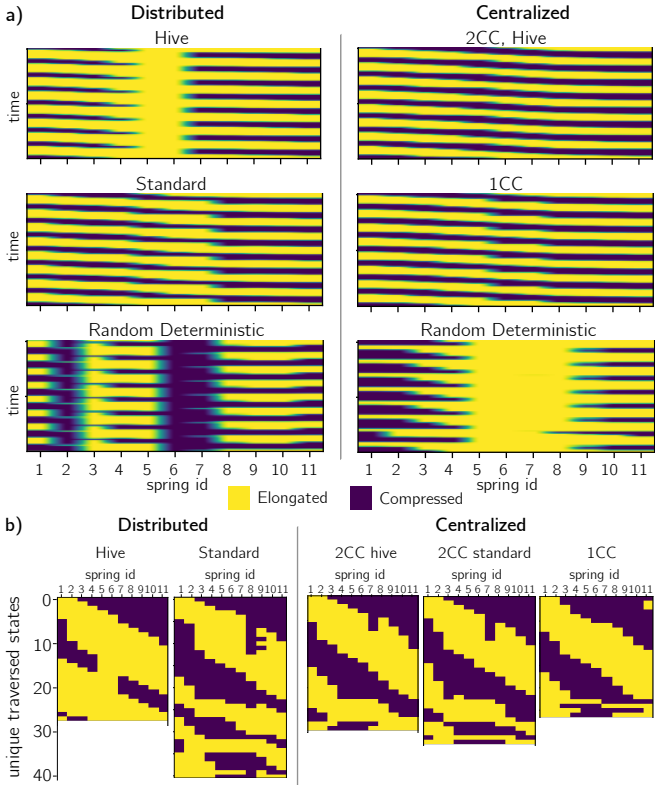


FIG. 6: Spring states observed when playing the best policy for the different architectures considered in the 12 suckers crawler, compared to a random deterministic policy. a) Kymographs of states experienced by each spring (x axis) during integration: each row corresponds to a different time; time increases on the y axis from top to bottom. b) Unique binary states of compression/elongation of the 11 springs experienced as the crawler adopts specific policies. Ordering of the states is chosen to guide the eye – it does not account for the time spent in each state nor the temporal order these states are encountered.

despite the lack of a direct measure of space or time. To characterize this intuition, we visualize kymographs of the state of compression of the springs generated by the dynamics as a crawling policy is enacted (fig. 6(a)). Note that the state of compression of the springs is not deterministically controlled by the adhesion pattern of the suckers. We find that all optimal policies generate periodic states of compression as seen by repeating patterns representing traveling waves of compression with speed ≈ 0.19108 , perfectly matching the underlying central pattern generator phase velocity, $v_p/x_0 = \omega/k \approx 0.19099$, with $\omega = 0.1$, $k = 2\pi/N_s$ and $N_s = 12$. This is in contrast to random deterministic policies, which generate random states of compression of the springs and cannot reproduce the CPG wave (bottom panel of fig. 6(a)). Interestingly, for distributed architectures and especially in the hive case the bands abruptly end near the center of the crawler, signifying that when the compression

wave hits springs 5 and 6 it stops: a clump of springs near the center of the crawler remains constantly elongated. In contrast, for centralized architectures the wave never stops but rather travels along the crawler all the way to the end, so that the CPG movement is effectively transferred to the crawling. Thus by orchestrating adhesion of multiple suckers at a time, centralized architectures realize a smoother traveling wave of compression. Consistently, when enacting optimal centralized policies, the dynamics generates a limited number of compression states. For the optimal fully centralized policy (1CC), the 12 springs experience only 26 states of compression, about 1% of the available 2^{N_s-1} combinations of binary states associated to the $N_s - 1$ springs. Interestingly, with distributed architectures the number of states visited using optimal policies is about 100% of the available $4(N_s - 1)$ states (fig. 6(b), standard).

IV. DISCUSSION AND PERSPECTIVES

Here we presented a toy model of a one dimensional crawler composed of blocks connected by springs. Each block is a rudimentary actuator representing a sucker making a single binary decision at each time: adhere *vs* not-adhere. The suckers are also rudimentary proprioceptors, as they measure the binary state of compression *vs* elongation of their adjacent springs. Positional information and speed of the individual suckers is not measured nor inferred. We assume that a central pattern generator, or CPG, periodically modifies the rest length of the springs, according to a traveling wave. Using this toy model we have demonstrated that this group of rudimentary proprioceptors/actuators can learn to interact with the substrate and exploit the wave generated by the CPG to achieve a net unidirectional motion of the crawler. Particularly, we focused on the pros and cons of distributed *vs* centralized forms of learning and control. Using tabular Q-learning, we found that locomotion can be learned in a pure multiagent setting, where each sucker is considered an independent agent and with no explicit communication among agents, consistent with previous literature [14]. In this setting, coupling is learned and is mediated by reward, as all suckers contribute to the dynamics that displaces the center of mass which produces reward. A purely distributed form of learning and control is cost effective in that it requires no communication and thus scales well with the number of agents and the degrees of freedom in the system.

We find that introducing a certain degree of centralization, in the form of Control Centers encompassing several suckers, provides two benefits. On the one hand, the increased complexity of centralized policies can be effectively exploited to couple the actions of many suckers at a time. These long range correlations enable centralized policies to more effectively ride the wave of compression provided by the CPG, and ultimately yield faster crawling. On the other hand, as multiple suckers are activated

at a time, failure of an individual sucker results in less dramatic loss of performance, making centralized policies both more effective and more robust to failure.

Centralization of course comes at the cost of increased computational cost and requires two-way communication of proprioceptive input from the suckers to the control center, and of motor control from the control center to the suckers. We find that intermediate architectures where multiple control centers orchestrate the actions of a subset of suckers achieve the best of both worlds, providing virtually identical benefits of full centralization, but limiting the number of degrees of freedom to a manageable size. Ultimately, partial or full centralization overcome the limits of binary proprioception and activation by realizing smooth and continuous dynamics, despite binary input and output. Further work is needed to establish the optimal degree of centralization, emerging from the trade-offs between robustness, speed and computational cost, which will be relevant to understand the control architecture of biological crawlers and to design efficient robotic crawlers (see e.g. [22, 23]).

Although the physics underlying crawling is clearly deterministic, the learning task is stochastic due to partial observability. Indeed, the deterministic dynamics of the crawler is dictated by the instantaneous positions and speeds of all suckers and rest length of all springs, but these are unknown to the agent. On top of this, in all but the fully centralized architecture, the individual agents are unaware of other agent’s actions and states of compression, which yields another source of stochasticity. In the context of partial observability, stochastic policies may provide better performance (e.g. adopting policy gradient methods) [16, 24]. More refined forms of Q-learning may also be beneficial here, for example double Q-learning which was reported to be more robust when dealing with stochastic Markov Decision Processes [25] or other modern RL-techniques, for instance based on Deep-RL which couples Neural Networks to Q-learning [16, 18, 26]. Some of these techniques may prove more effective than our simple approach based on tabular Q-learning. However they remain outside the scope of the present paper where we focused on disentangling the benefits and limits of distributed *vs* centralized learning architectures. For example, a complex neural network naturally couples inputs and outputs and may thus not be the natural choice to parse the role of centralization *vs* distribution.

In contrast, previous biologically inspired work focused on either a fully centralized [13] or fully distributed (hive) control [14]. In [13], a biologically plausible model of crawling is proposed which also uses rudimentary forms of proprioception and control: input is limited to the identity of the most compressed body segment and actions correspond the designation of the sole active neuron in the neural network controlling muscular contraction, while adhesion is not controlled. The authors show with a fully centralized Q-learning architecture that the central pattern generator can be learned, rather than imposed

as we do here.

In [14], swimming of an agent is achieved through training of a genetic algorithm with a fully distributed architecture, where individual actuators are all forced to learn the same policy – which we have called hive update here. Again, the actuators are not suckers but rather beads which control the restoring force between their neighbors. The hive update was found to generalize well to a different number of beads, with no need for re-training. This is consistent with our finding, where we also observe that the hive update almost invariably learns the same policy, independent on the number of suckers composing the crawler. However, while we focus on binary sensing and control, Ref. [14] considers actuators with full proprioception, including the position and speeds of their neighbors. An advantage of considering binary proprioception is its simple implementation and interpretation. For example, our hive update can be understood in simple terms: suckers learn to only adhere when they are pushed and pulled backward from both sides.

Here we have focused on the learning process that enables suckers to achieve crawling by combining mechanical contractions and interaction with the substrate. In our model, thrust is achieved by letting suckers control patterns of adhesion to the solid substrate, whereas contraction results from the stereotypic wave of compression and the dynamics. In refs. [13, 14] switch the controls: the actuators learn patterns of contraction, and interaction with their solid and fluid environment respectively is embedded in the dynamics. Finally, in bio-inspired models of sea star locomotion [6, 7], thrust is achieved by fully prescribing –rather than learning– actions. Synchronization here emerges through the dynamical interaction of the substrate with the tube feet, which are physically connected to the body, with a mechanism reminiscent of the Kuramoto model of synchronization [27, 28].

Here we parsed the pros and cons of distribution *vs* centralization for learning the internal coordination among body parts, aimed at translocation. The benefits of centralization for speed and robustness point to a potential origin of selective pressure towards more centralized forms of nervous systems. To what extent early nervous systems allowing the Cambrian explosion may have emerged from the need for internal coordination *vs* from the need of processing complex sensory information is currently debated, see e.g. [29–31]. Our results are dictated purely by the need to internally coordinate body parts to generate thrust, but the role of centralization may become even more prominent when sensation and locomotion are coupled to aim toward a specific target. Indeed, this requires that each unit senses not only the internal state of compression of the organism, but also sensory signals from the environment, from e.g. vision, audition, taste and olfaction. Our approach may be further extended to sensory navigation, by enriching the state definition with sensory cues from the environ-

ment and rewarding not only speed but also the successful reaching of a sensory target.

Our model is inspired by octopuses and other cephalopods, organisms with a distributed nervous system whose proprioception remains elusive [11, 32]. Control centers coordinating adhesion of a few suckers with rudimentary proprioception achieves fast translocation without incurring into the computational cost of a fully centralized brain. Our approach may be further developed to quantify performance, robustness and computational cost as a function of the number of control centers, to select an “optimal” number of control centers for crawling, aimed at both fast locomotion as well as sensory navigation toward a target. Control centers may be adapted to model how ganglia distributed along the arms of an octopus control locomotion. To what extent the robustness, performance and computational cost of crawling shape the connectivity of the ganglia distributed along the octopus arms’ and the organization of their taste-by-touch sensory system [8, 33, 34] is an exciting avenue for further research.

ACKNOWLEDGMENTS

This research was supported by grants to Agnese Seminara from the European Research Council (ERC) under the European Union’s Horizon 2020 research and innovation programme (grant agreement No 101002724 RIDING) and the National Institutes of Health (NIH) under award number R01DC018789. This work represents only the view of the authors. The European Commission and the other funding agencies are not responsible for any use that may be made of the information it contains.

Appendix A: Materials and Methods

1. Equation of motion

Referring to the definitions introduced in the main text and fig. 1, the general differential equation governing the internal blocks (excluding tail and head) is given by

$$m\ddot{x}_n(t) = -\zeta_n \dot{x}_n(t) + \kappa(x_{n+1}(t) - x_n(t) - l_n(t)) - \kappa(x_n(t) - x_{n-1}(t) - l_{n-1}(t)) \quad (\text{A1})$$

where x_n is the position of the n th sucker, with $n = 1, \dots, N_s - 1$. For the tail, $n = 0$, and the head, $n = N_s$, the dynamics is given by:

$$m\ddot{x}_0(t) = -\zeta_0 \dot{x}_0(t) + \kappa(x_1(t) - x_0(t) - l_0(t)) \quad (\text{A2})$$

$$m\ddot{x}_{N_s}(t) = -\zeta_{N_s} \dot{x}_{N_s}(t) - \kappa(x_{N_s}(t) - x_{N_s-1}(t) - l_{N_s-1}(t)) \quad (\text{A3})$$

2. Scaling and parametrization

Recalling the CPG equation eq. (1), $l_n = x_0 + a \sin(\omega t - kn)$, being x_0 the rest position of each spring, it fixes the spatial scaling of the problem. Introducing the rescaled position of the suckers/block, $\bar{x} = x/x_0$, $\bar{l} = l/x_0$, and the constants $A = m/(\zeta_0 \omega^2)$ and $B = \kappa/(\zeta_0 \omega)$, the above equations can be rewritten as:

$$\begin{aligned} A\ddot{\bar{x}}_n(t) &= -\dot{\bar{x}}_n(t) + B(\bar{x}_{n+1}(t) + \bar{x}_{n-1}(t) - 2\bar{x}_n(t) - \bar{l}_n(t) + \bar{l}_{n-1}(t)) \\ A\ddot{\bar{x}}_0(t) &= -\dot{\bar{x}}_0(t) + B(\bar{x}_{n+1}(t) - \bar{x}_n(t) - \bar{l}_n(t)) \\ A\ddot{\bar{x}}_{N_s}(t) &= -\dot{\bar{x}}_{N_s}(t) + B(\bar{x}_{N_s-1}(t) - \bar{x}_{N_s}(t) + \bar{l}_{N_s-1}(t)) \end{aligned} \quad (\text{A4})$$

In the following, we assume the overdamped limit, that is the inertial term is negligible compared to the other terms, $A \ll B$. Therefore the differential equation representing the dynamics of the n th internal crawler in absence of adhesion simplifies to a cinematic equation:

$$\dot{\bar{x}}_n(t) = B(\bar{x}_{n+1}(t) + \bar{x}_{n-1}(t) - 2\bar{x}_n(t) - \bar{l}_n(t) + \bar{l}_{n-1}(t)) \quad (\text{A5})$$

When the n th suckers is adhering to the substrate ($\zeta_n = \infty$) $B = 0$, we simply have null instantaneous velocity, $\dot{\bar{x}}_n = 0$. We think that the overdamped approximation is reasonable for the purpose of this work. In Appendix B.2, for validation purposes, we show the damped dynamics already approaching the overdamped limit when the ratio between inertia and friction is of order one, $m/\zeta_0 = 1$. The spatial periodicity N in the CPG oscillation is in principle an arbitrary integer. For simplicity, we fix N identical to the number of suckers, N_s , so that a single wavelength, $\lambda = Nx_0$, is contained in the crawler. Therefore, given the crawler length L , we have $\lambda = L$ and x_0 is scaled according to the number of suckers considered, $x_0 = L/N_s$. Other parameters are fixed to $\kappa = 1 \text{ N/m}$, $\zeta_0 = 1 \text{ N/m}$, $\omega = 0.1 \text{ s}^{-1}$, $a = x_0/4$ (the amplitude of the oscillation of the CPG), and $L = 10 \text{ m}$. To summarize

the problem is dictated by 3 nondimensional parameters, $N_s = L/x_0$, L/λ and $B = \kappa/(\zeta_0\omega)$:

$$\begin{cases} B &= 10 \\ L/\lambda &= 1 \text{ except for fig. 11} \\ N_s &\text{varying} \end{cases} \quad (\text{A6})$$

Appendix B: Validation

1. Periodic crawler



FIG. 7: Sketch of the periodic crawler model.

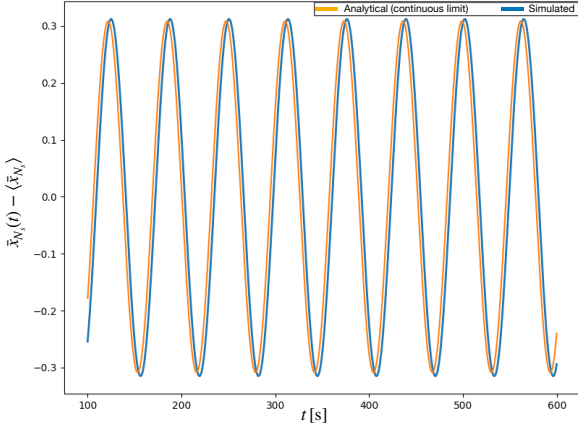


FIG. 8: For validation purposes, we here track the movement of the head of a 10 suckers crawler in overdamped dynamics and with periodic boundary conditions (infinite crawler ideal model) and compare it to the analytical solution of eq. (B1). The position are reported in the reference frame of the time-averaged position and in normalized units $\bar{x} = x/x_0$. The amplitude of the oscillation is here $a = x_0/3$.

As discussed in [15], in the continuous limit the equilibrium spring position (central pattern generator) is $l(s, t) = x_0 + a \sin(\omega t - ks)$, with $s = nx_0$, $k_c = 2\pi/\lambda$ and $\lambda = Nx_0$ with N the periodicity. It can be proven [15] that without any perturbation, i.e. no adhesion, that is uniform and constant friction across all the crawler, ζ_0 , the continuous equation of motion for a sucker at location s is

$$u^0(s, t) = C \cos(\omega t - k_c s - \theta) \quad (\text{B1})$$

with $\theta = \tan^{-1} \tilde{\omega}$, $\tilde{\omega} = \zeta_0 \omega / (k^2 \kappa)$, with κ the springs elastic constant, and $C = a/N \cos \theta$. We can approach the

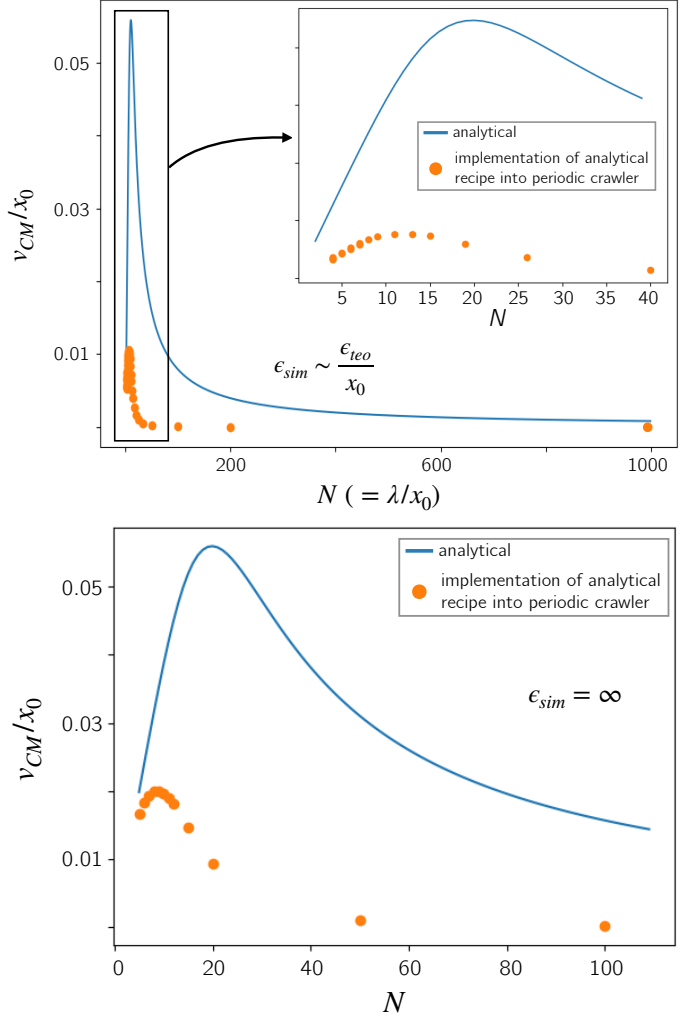


FIG. 9: Comparison between eq. 4.9 of [15] (eq. (4) in the main text without constant prefactors) (blue lines), and the implementation of eq. (3) in the simulator (orange dots) for the periodic crawler model. a) A more honest comparison with the perturbation regime used in Ref. [15] which accounts for the small adhesion limit, using $\epsilon = 1$ in the simulator. b) With infinite adhesion in the simulator as the one used generally in this work.

system described in [15], where they assume an infinite crawler, by considering a discrete crawler with periodic boundary conditions and check how the unperturbed solution (no sucker adhering) compares to the analytical prediction of eq. (B1). As illustrated in fig. 7, periodic boundary conditions are implemented by considering a virtual replica of the tail connected to the last right-hand sucker of the crawler. The comparison is made in fig. 8 where we track the head position of the simulated periodic crawler with no adhesion (so no net movement of the center of mass, $v_{CM} = 0$). The comparison is extremely good with what predicted from theory.

However, when the crawler is perturbed by the adhesion pulse of eq. (3), the perturbative analytical solution

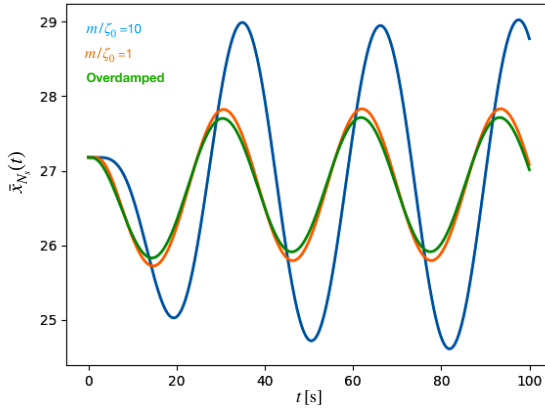


FIG. 10: head position as a function of the integration time in scaled units $\bar{x} = x/x_0$. The damped regime collapses on the overdamped limit for values of the scaled constant $A\omega^2 = m/\zeta_0 < 1$ in eq. (A4), where the overdamped dynamics is given by eq. (A5).

proposed by [15], we are probably bounded in the comparison by the impossibility of realizing a genuine continuous limit and an infinite tentacle. Indeed, as shown in fig. 9, the implementation of the optimal crawling strategy of eq. (3) in the periodic crawler model discussed in this appendix, does not compare well to the perturbation analysis leading to eq. (4).

However, as also shown in the Results section for the finite crawler, we have a fairly good qualitative comparison with the theoretical behavior, namely the existence of a maximum in N ($= N_s$, the number of suckers for our parametrization), and a decay for $N \rightarrow \infty$. The position of the maximum is not exactly the one predicted by the analytical theory but similar (with $\omega = 0.1$, $N_{\max}^{\text{finite}} \sim 12 < \tilde{N}_{\max} = (2\pi)/\sqrt{\omega} = 20$). Interestingly, as illustrated by fig. 3 in the main text, the functional shape of the dependency with N_s is preserved even when crawling policies allow for the adhesion of multiple suckers at a time which was excluded from the analytical treatment of Ref. [15].

2. Damped limit

For validation purposes, we can drop the overdamped assumption and solve the full damped equation for the finite crawler eq. (A4). In fig. 10, we show that the overdamped regime is already approached when the mass of the "sucker block" and the friction coefficient are of the same order. Preliminary results also suggest that policies learned in the damped regime are no significantly different from the overdamped ones. Therefore, we expect that the conclusions reached in this work should still hold in the damped scenario. However, further verifica-

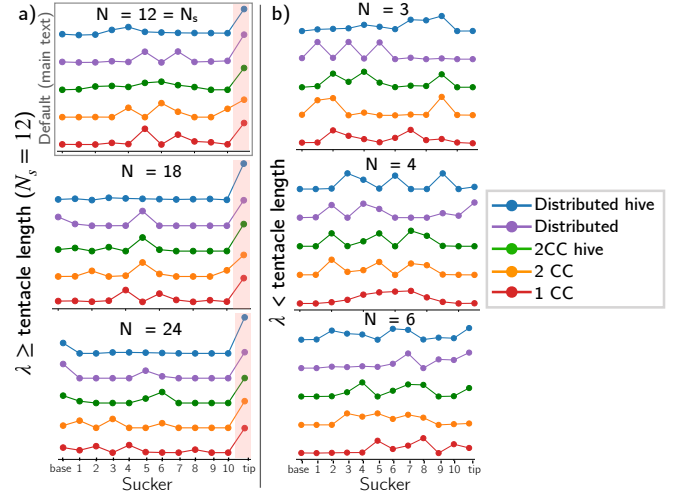


FIG. 11: Effect of different wave forms of the CPG over the first order sucker importance for a $N_s = 12$ suckers crawler. We can note that when the wavelength is equal or larger than the crawler length, $N \geq N_s$, the head is always the most impactfull sucker for all the considered learning architectures. This invariance does not hold anymore when $\lambda < L$.

tions would be needed to assert this claim unequivocally.

Appendix C: Effect of CPG periodicity over sucker importance

In this work in general we assume for simplicity that a single wavelength is contained in the crawler, $\lambda = L$ (that is, $N = N_s$). As discussed in the main text, we found that when playing a crawler policy the head is on average the most impactfull sucker upon failures, whatever the considered learning architecture. To establish if this is a general property and how it correlates to the physics of the system, we analyzed for the 12 suckers system how this property is affected when dropping the assumption that the CPG wavelength, λ , is identical to the crawler length, L . The results, shown in fig. 11, indicate that the head is always the most determinant sucker only when the CPG wavelength is $\lambda \geq L$. However, when $\lambda < L$ we cannot find a single sucker to be the most important for all the considered architecture, but its identity varies with the considered policy (architecture) and wavelength. We do not have yet a definite explanation of this phenomenon, but this results already indicates a non-trivial interplay between the underlying physic of crawling, namely the (discrete) placement of each sucker with respect to the CPG, and crawling policies.

-
- [1] W. N. Frost, *Current Biology* **33**, R398 (2023), ISSN 09609822.
- [2] J. Bielecki, S. K. Dam Nielsen, G. Nachman, and A. Garm, *Current Biology* **33**, 4150 (2023), ISSN 09609822.
- [3] C. A. Freas and K. Cheng, *Learning & Behavior* **50**, 20 (2022), ISSN 1543-4494, 1543-4508.
- [4] T. Kano, D. Kanauchi, H. Aonuma, E. G. Clark, and A. Ishiguro, *Frontiers in Neurorobotics* **13**, 66 (2019), ISSN 1662-5218.
- [5] E. G. Clark, D. Kanauchi, T. Kano, H. Aonuma, D. E. G. Briggs, and A. Ishiguro, *Journal of Experimental Biology* p. jeb.192104 (2018), ISSN 1477-9145, 0022-0949.
- [6] T. Po, E. Kanso, and M. J. McHenry, *Current Biology* **34**, 2551 (2024), ISSN 09609822.
- [7] S. Heydari, A. Johnson, O. Ellers, M. J. McHenry, and E. Kanso, *Journal of The Royal Society Interface* **17**, 20190700 (2020), ISSN 1742-5689, 1742-5662.
- [8] C. A. Allard, W. A. Valencia-Montoya, and N. W. Bellono, *Current Biology* **33**, R1081 (2023), ISSN 09609822.
- [9] J. A. Mather and L. Dickel, *Current Opinion in Behavioral Sciences* **16**, 131 (2017), ISSN 23521546.
- [10] G. Levy, T. Flash, and B. Hochner, *Current Biology* **25**, 1195 (2015), ISSN 09609822.
- [11] T. Gutnick, R. A. Byrne, B. Hochner, and M. Kuba, *Current Biology* **21**, 460 (2011), ISSN 09609822.
- [12] L. Zullo, G. Sumbre, C. Agnisola, T. Flash, and B. Hochner, *Current Biology* **19**, 1632 (2009), ISSN 09609822.
- [13] S. Mishra, W. M. Van Rees, and L. Mahadevan, *Journal of The Royal Society Interface* **17**, 20200198 (2020), ISSN 1742-5689, 1742-5662.
- [14] B. Hartl, M. Levin, and A. Zöttl, *Communications Physics* **8**, 194 (2025), ISSN 2399-3650.
- [15] Y. Tanaka, K. Ito, T. Nakagaki, and R. Kobayashi, *Journal of The Royal Society Interface* **9**, 222 (2012), ISSN 1742-5689, 1742-5662.
- [16] R. S. Sutton and A. Barto, *Reinforcement Learning: An Introduction*, Adaptive Computation and Machine Learning (The MIT Press, Cambridge, Massachusetts London, England, 2020), second edition ed., ISBN 978-0-262-03924-6.
- [17] J. K. Terry, N. Grammel, S. Son, B. Black, and A. Agrawal, *Revisiting Parameter Sharing in Multi-Agent Deep Reinforcement Learning* (2023), 2005.13625.
- [18] A. Plaat, *Deep Reinforcement Learning* (Springer Nature Singapore, Singapore, 2022), ISBN 978-981-19063-7-4 978-981-19063-8-1.
- [19] D. L. Young and C. Eccles, in *Artificial Intelligence and Machine Learning for Multi-Domain Operations Applications II*, edited by T. Pham, L. Solomon, and K. Rainey (SPIE, Online Only, United States, 2020), p. 44, ISBN 978-1-5106-3603-3 978-1-5106-3604-0.
- [20] S. Mahadevan, *Machine Learning* **22**, 159 (1996), ISSN 0885-6125, 1573-0565.
- [21] L. Gagliardi, *Git repo: Control a 1D Crawler*. https://github.com/PimLb/control_1D_crawler.git (2025).
- [22] S. Chen, Y. Cao, M. Sarparast, H. Yuan, L. Dong, X. Tan, and C. Cao, *Advanced Materials Technologies* **5**, 1900837 (2020), ISSN 2365-709X, 2365-709X.
- [23] T. Sato, W. Watanabe, and A. Ishiguro, in *2010 IEEE International Conference on Robotics and Automation* (IEEE, Anchorage, AK, 2010), pp. 709–714, ISBN 978-1-4244-5038-1.
- [24] J. Peters and S. Schaal, *Neural Networks* **21**, 682 (2008), ISSN 08936080.
- [25] H. V. Hasselt, *Advances in Neural Information Processing Systems* **23** (2010).
- [26] M. Kim, J.-S. Kim, M.-S. Choi, and J.-H. Park, *Sensors* **22**, 7266 (2022), ISSN 1424-8220.
- [27] Y. Kuramoto, in *International Symposium on Mathematical Problems in Theoretical Physics*, edited by H. Araki (Springer-Verlag, Berlin/Heidelberg, 1975), vol. 39, pp. 420–422, ISBN 978-3-540-07174-7.
- [28] S. H. Strogatz, *Physica D: Nonlinear Phenomena* **143**, 1 (2000), ISSN 01672789.
- [29] G. Jékely, F. Keijzer, and P. Godfrey-Smith, *Philosophical Transactions of the Royal Society B: Biological Sciences* **370**, 20150181 (2015), ISSN 0962-8436, 1471-2970.
- [30] D. Arendt, M. A. Tosches, and H. Marlow, *Nature Reviews Neuroscience* **17**, 61 (2016), ISSN 1471-003X, 1471-0048.
- [31] F. Keijzer and A. Arnellos, *Biology & Philosophy* **32**, 421 (2017), ISSN 0169-3867, 1572-8404.
- [32] M. J. Wells, *Journal of Experimental Biology* **37**, 489 (1960), ISSN 0022-0949, 1477-9145.
- [33] H. Bagheri, A. Hu, S. Cummings, C. Roy, R. Casleton, A. Wan, N. Erjavić, S. Berman, M. M. Peet, D. M. Aukes, et al., *Advanced Intelligent Systems* **2**, 1900154 (2020), ISSN 2640-4567, 2640-4567.
- [34] L. Van Giesen, P. B. Kilian, C. A. Allard, and N. W. Bellono, *Cell* **183**, 594 (2020), ISSN 00928674.